Elsevier Editorial System(tm) for Acta Materialia
Manuscript Draft

Manuscript Number: A-12-785R1

Title: Phase relations and optoelectronic characteristics in the NdVO4-BiVO4 system

Article Type: Full Length Article

Keywords: Photocatalysis; Orthovanadates; Solid solution; Extended X-ray absorption fine structure; Optical spectroscopy.

Corresponding Author: Ms. Mirela Dragomir,

Corresponding Author's Institution: University of Nova Gorica

First Author: Mirela Dragomir

Order of Authors: Mirela Dragomir; Iztok Arčon; Sandra Gardonio; Matjaz Valant

Abstract: Studies performed on NdVO4-BiVO4 system showed on existence of the BixNd1−xVO4 homogeneity range for $x \leq 0.49(1)$. EXAFS and XRD analyses confirmed that Bi3+ incorporates onto the Nd site in the NdVO4 crystal structure with some distortion of the local structure. Surprisingly, the unit cell volume decreases with the increase in the content of the larger Bi3+ ion. On the other side of the NdVO4-BiVO4 system, Nd3+ does not enter the BiVO4 structure but forms the NdVO4-based secondary phase. UV-Vis spectroscopy showed that the band gap of NdVO4 can be reduced to below 3.1 eV by the Bi-doping. New emissions that do not exist for NdVO4 have been found in the 650-675 nm range of BixNd1−xVO4 photoluminescence spectra. The observed chemical and optoelectronic properties were explained on the basis of the hybridization of Bi 6s2 and O 2p orbitals.

Nova Gorica, September 27th, 2012

Dear Editor,

Thank you for your useful comments and suggestions on our manuscript (Ms. No. A-12-785) entitled: **'Phase relations and optoelectronic characteristics in the $NdVO_4$-$BiVO_4$ system'** by M. Dragomir, I. Arčon, S. Gardonio, and M. Valant. We carefully considered all the comments and modified the manuscript accordingly. Herein, we explain how we revised the paper based on those comments and recommendations.

Comment no. 1: *The English composition does not meet Acta Materialia standards; it is imperative that you have this paper thoroughly edited by someone well versed in the English language.*

Response: A skilled author of English papers has revised the whole manuscript carefully and we believe that the language is significantly improved.

Comment no. 2: *Figures 4,5,6 and 7 in the manuscript have no error bars to indicate the confidence you have in the accuracy of each datum point. As outlined in the journal's stated instructions, these error bars should be inserted in the figures and discussed in the text if necessary. If the error bars are such that they would not be visible on the scale of the diagram as presented, then please indicate so in the text and justify this fact.*

Response: The measurement error corresponding to the figures 4, 5, 6, and 7 have been discussed in the text and the error bars inserted in the figures.

Reviewer no. 1:

Comment no. 1. *This paper represents a thorough and well-executed study on the properties of the $BiVO_4$-$NdVO_4$ solid solution system. It provides new insights into the intricacies of A-*

site doping of both end-members, something which is very important for photocatalytic (and perhaps also other) applications. My only major comment on this paper concerns the extrapolation procedure used in the UV/VIS optical spectra in Figs. 8 and 9. The authors extrapolate the graph to the x-axis of the graph; this corresponds to a negative absorption (!), and is therefore clearly in error. Instead, the plotted data between 1.5 - 2.3 eV (inset Fig 8) and 1.6 - 2.2 eV (inset Fig 9) should be linearly extended and used as a baseline for the bandgap determination. This will result in slightly larger bandgap values for both materials.

Response: The comments were very useful and we have corrected the figures and the values of the band gaps accordingly: the data between 1.5–2.3 eV (inset Fig 8) and 1.6–2.2 eV (inset Fig 9) were linearly extended and used as a baseline for the band gap determination. Indeed, this resulted in slightly larger band gaps for both cases.

Comment no. 2. *A minor comment: on page 3 (bottom), the authors refer to the BiVO4 / metal junction as a heterojunction. The word "heterojunction" is usually reserved for a junction between two (different) semiconductors. I therefore suggest to change this sentence to "... better electron-hole separation near the formed metal-semiconductor junctions".*

Response: We have changed the word *'heterojunctions'* with *'metal-semiconductor junctions'* as the Reviewer no.1 suggested.

In addition, we have checked again that only SI units of measurement were used throughout our paper. The corrected version of the manuscript has been resubmitted to your journal.

Again, we appreciate all your comments. We hope that these revisions improved the paper such that you and the reviewer deem it worthy of publication in Acta Materialia.
Thank you for your time and consideration.

Sincerely,
Mirela Dragomir (for all the co-authors)

Nova Gorica, September 27th, 2012

Dear Reviewer,

Thank you for your useful comments and suggestions on our manuscript (Ms. No. A-12-785) entitled: **'Phase relations and optoelectronic characteristics in the $NdVO_4$-$BiVO_4$ system'** by M. Dragomir, I. Arčon, S. Gardonio, and M. Valant. We carefully considered all the comments and modified the manuscript accordingly. Herein, we explain how we revised the paper based on those comments and recommendations.

Comment no. 1. *This paper represents a thorough and well-executed study on the properties of the $BiVO_4$-$NdVO_4$ solid solution system. It provides new insights into the intricacies of A-site doping of both end-members, something which is very important for photocatalytic (and perhaps also other) applications. My only major comment on this paper concerns the extrapolation procedure used in the UV/VIS optical spectra in Figs. 8 and 9. The authors extrapolate the graph to the x-axis of the graph; this corresponds to a negative absorption (!), and is therefore clearly in error. Instead, the plotted data between 1.5 - 2.3 eV (inset Fig 8) and 1.6 - 2.2 eV (inset Fig 9) should be linearly extended and used as a baseline for the bandgap determination. This will result in slightly larger bandgap values for both materials.*

Response: The comments were very useful and we have corrected the figures and the values of the band gaps accordingly: the data between 1.5–2.3 eV (inset Fig 8) and 1.6–2.2 eV (inset Fig 9) were linearly extended and used as a baseline for the band gap determination. Indeed, this resulted in slightly larger band gaps for both cases.

Comment no. 2. *A minor comment: on page 3 (bottom), the authors refer to the BiVO4 / metal junction as a heterojunction. The word "heterojunction" is usually reserved for a junction between two (different) semiconductors. I therefore suggest to change this sentence to "... better electron-hole separation near the formed metal-semiconductor junctions".*

Response: We have changed the word *'heterojunctions'* with *'metal-semiconductor junctions'* as the Reviewer no.1 suggested.

Again, we appreciate all your comments. We hope that these revisions improved the paper such that you deem it worthy of publication in Acta Materialia.
Thank you for your time and consideration.

Sincerely,
Mirela Dragomir (for all the co-authors)

Phase relations and optoelectronic characteristics in the $NdVO_4$-$BiVO_4$ system

Mirela Dragomir[a,1], Iztok Arčon[a,b,c], Sandra Gardonio[a], Matjaz Valant[a,d]

[a]*University of Nova Gorica, 5000 Nova Gorica, Slovenia*
[b]*Jozef Stefan Institute, Jamova 39, SI-1000 Ljubljana, Slovenia*
[c]*CO-NOT, Hajdrihova 19, SI-1000, Ljubljana, Slovenia*
[d]*Center of Excellence for Biosensors, Instrumentation and Process Control, 5250 Solkan, Slovenia*

Abstract

Studies performed on $NdVO_4$-$BiVO_4$ system showed on existence of the $Bi_xNd_{1-x}VO_4$ homogeneity range for $x \leq 0.49(1)$. EXAFS and XRD analyses confirmed that Bi^{3+} incorporates onto the Nd site in the $NdVO_4$ crystal structure with some distortion of the local structure. Surprisingly, the unit cell volume decreases with the increase in the content of the larger Bi^{3+} ion. On the other side of the $NdVO_4$-$BiVO_4$ system, Nd^{3+} does not enter the $BiVO_4$ structure but forms the $NdVO_4$-based secondary phase. UV-Vis spectroscopy showed that the band gap of $NdVO_4$ can be reduced to below 3.1 eV by the Bi-doping. New emissions that do not exist for $NdVO_4$ have been found in the 650-675 nm range of $Bi_xNd_{1-x}VO_4$ photoluminescence spectra. The observed chemical and optoelectronic properties were explained on the basis of the hybridization of Bi $6s^2$ and O 2p orbitals.

Keywords

Photocatalysis; Orthovanadates; Solid solution; Extended X-ray absorption fine structure; Optical spectroscopy.

[1]Corresponding author. E-mail: mirela.dragomir@ung.si. Postal address: Vipavska 11c, 5270 Ajdovscina, Slovenia. Tel.: +386 5 365 35 39, fax:+386 5 365 35 27

1. Introduction

Efficient use of solar energy still remains a challenge due to the lack of a stable and efficient visible-light active photocatalyst [1,2]. Most of photocatalytic materials, developed so far, are wide-band gap semiconductors (e.g. TiO_2, $SrTiO_3$, WO_3 etc) active only under ultraviolet (UV) light [3–6]. For an effective use of sunlight several different techniques for tuning their optoelectronic properties towards the visible spectral range have been developed, e.g. band gap engineering by doping [2,7], use of co-catalysts [8], and sensitizers [9] etc. Another approach is development of new, more effective, narrow-band gap semiconducting materials.

Monoclinic $BiVO_4$ (with a distorted scheelite structure, space group I2/b, also called *fergusonite)* has been recognized to be an efficient, chemically stable, visible-light active photocatalytic material [10,11]. Two other polymorphs of $BiVO_4$ are known: tetragonal dreyerite (zircon-type structure, space group $I4_1/amd$) and tetragonal scheelite (space group $I4_1/a$). The monoclinic scheelite-type phase undergoes a reversible second-order transition to the tetragonal scheelite structure at about 528 K [12-14]. This phase transition has been found to be driven by a small lone pair distortion on the Bi^{3+} ion [13]. A metastable tetragonal zircon-type $BiVO_4$ phase undergoes an irreversible transformation to the monoclinic scheelite-type on heating at 670–770 K [14], or by mechanical stress [12]. The different $BiVO_4$ polymorphs have different absorption characteristics and, consequently, their photocatalytic activities differ significantly. For instance, the tetragonal $BiVO_4$ with a band gap of 2.9 eV shows the absorption band in the near UV [15], while the monoclinic form with a band gap of 2.4 eV shows the absorption band in the visible region [15–17]. $BiVO_4$ in the monoclinic form is a well-known chemically stable and nontoxic visible-light photocatalyst with an excellent

photocatalytic activity that is attributed to its narrow band gap and large bandwidths [18]. In conventional metal oxide semiconductors, the top of the valence band is solely contributed by O 2p orbitals resulting in a wide band gap, but in the case of the monoclinic $BiVO_4$, the Bi $6s^2$ lone pair electrons create hybridized orbitals with O 2p orbitals [19,20], which leads to an up-shift of the top of the valence band, while the bottom of the conduction band remains unaffected due to its V 3d nature. Furthermore, the low effective mass of electrons and holes [18–20] and high energy dispersion in the band structure of $BiVO_4$ [18] significantly improve separation and transport properties of the photoexcited charges. $BiVO_4$ is known to be a good photocatalyst for the degradation of organic dyes [11,21] and a stable oxygen evolution catalyst in the presence of sacrificial electron acceptors (such as Ag^+) [10,21]. But it is catalytically inactive for hydrogen evolution due to its too low conduction band position relative to the proton reduction potential. Even though $BiVO_4$ has the unsuitable band position for hydrogen evolution, the overall water splitting reaction can still be achieved by using a separate hydrogen evolution catalyst in tandem (Z-scheme) [22]. Although the monoclinic $BiVO_4$ exhibits very interesting optoelectronic properties, its photocatalytic activity is still low. A shaped-controlled synthesis of $BiVO_4$ particles has been proven to be an efficient way to increase its photocatalytic activity [11,21,23]. Another way to enhance the photocatalytic performance of $BiVO_4$ is by doping or metal loading. Loading with noble metals such as Pt [24], Pd [25], Au [26], Ag [27] or with transitional metals, such as Co [27–29], Ni [27], Fe [30] or Cu [31], increased the photocatalytic activity of $BiVO_4$ by reducing the electron-hole recombination rate due to a better electron-hole separation near the metal-semiconductor junctions. A moderate B-site doping with Mo [32], W [33] or P [17] can improve the electron transport in

$BiVO_4$, while a recent study [34] reported that doping of $BiVO_4$ with Al is another efficient way to suppress the recombination of the excitons. No successful A-site doping of the monoclinic $BiVO_4$ has been reported so far with an exception of co-substitution of Bi and V with Ca and Mo [16], respectively, which converted the monoclinic unit cell to tetragonal. The isovalent A-site substitutions with rare-earths ions such as Ce [35], Eu [36,37], Gd [36], 8 at.% Nd [36], and Er [36,38] have not been successful. An XPS analysis has shown segregation of Eu_2O_3 and Gd_2O_3 on the surface of the monoclinic $BiVO_4$ particles, which has been the reason for the observed enhanced photocatalytic activity.

It has recently it been found that $NdVO_4$ (a wide band gap semiconductor with a zircon-type structure and $I4_1/amd$ space group [39]) exhibits a photocatalytic activity for degradation of dyes and organic pollutants which is comparable [40] or even higher than that of the commercial TiO_2 [41]. But due to its wide band gap (>3eV), $NdVO_4$ is an UV active material [42]. Reports on the doping of $NdVO_4$ have showed that the photocatalytic activity of $NdVO_4$ under UV and visible-light irradiation can be improved by B-site Mo-doping [43]. Such doping reduces the band gap and broadens the distribution of the density of states in the conduction band. However, the synthesis of Bi-doped $NdVO_4$ and the effect of Bi-doping on the structure and, consequently, on the electronic properties of neodymium orthovanadate has not yet been reported.

The aim of this study is to investigate phase relations and solid solution formation in the $NdVO_4$-$BiVO_4$ system and characterize the crystal structure and optoelectronic properties of the existing phases with X-ray diffraction (XRD) and extended X-ray absorption fine structure (EXAFS), diffuse reflectance (DRS), and photoluminescence (PL) spectroscopy techniques. For the solid solution between

$NdVO_4$ and $BiVO_4$ we can expect a reduction in the band gap of $NdVO_4$ through coupling between Bi $6s^2$ and O 2p orbitals, which would move the absorption towards the visible-light range and contribute to the higher photocatalytic activity. To optimize this bad gap modification, the substitution mechanisms and the extent of the homogeneity ranges have to be determined.

2. Experimental section

Bi-doped $NdVO_4$ with a nominal stoichiometry of $Bi_xNd_{1-x}VO_4$ (x = 0, 0.10, 0.40, 0.45, 0.48, 0.50, and 0.60) and Nd-doped $BiVO_4$ with a nominal stoichiometry of $Nd_yBi_{1-y}VO_4$ (y = 0, 0.05, 0.08, and 0.10) were prepared by the solid-state method. Stoichiometric amounts of Bi_2O_3 (Alfa Aesar, 99.975% purity), V_2O_5 (Alfa Aesar, 99.6% purity) and Nd_2O_3 (Alfa Aesar, 99.6% purity) were homogenized in a planetary mill using ethanol as a homogenizing medium. The powders were dried and pressed into pellets. The $Bi_xNd_{1-x}VO_4$ samples were calcinated in air in two steps, at 973 K for 3 h and 1073 K for 3 h. The $Nd_yBi_{1-y}VO_4$ samples were fired in air at 1073 K for 10 h.

The crystallographic characterization was carried out with x-ray powder diffraction using a PANalytical X-ray diffractometer with Cu K_α radiation (λ = 0.154 nm), a step size of 0.017° and scan step time of 25.8 s. The diffraction patterns were recorded in the range 2θ = 5-80°. Crystallite size calculation and the refinement of the unit cell were performed using the PANalytical X'pert HighScore Plus software.

Bi L_3-edge Nd L_3-edge and V K-edge EXAFS spectra were measured at C beamline of HASYLAB (Hamburg, Germany) in a transmission detection mode at room temperature, using a Si(311) double-crystal monochromator with ~1.5 eV resolution at the Bi L_3-edge (13419 eV), and Si(111) double-crystal monochromator with 1 eV

resolution at the Nd L_3-edge (6208 eV) and V K-edge (5465 eV). The higher-order harmonics were efficiently eliminated by detuning the monochromator crystals to 60% of the rocking curve maximum using a stabilization feedback control. The intensity of the X-ray beam was measured by three consecutive 10 cm long ionization detectors, the first filled with 190 mbar of Ar, and the second and third with 1000 mbar of Kr, for the Bi L_3-edge EXAFS, while for the Nd L_3-edge and V K-edge EXAFS the cells were filled with 520 mbar of N_2, 250 mbar of Ar, and 400 mbar of Ar, respectively. The samples were placed between the first two detectors. The exact energy calibration was obtained by an absorption measurement on Pb metal foil (Pb L_3-edge 13035 eV), or Bi metal foil and Ti metal foil (Ti K-edge 4966 eV) or V metal foil, inserted between the second and the third ionization detector. The samples were prepared in the form of homogeneous pellets with an absorption thickness of about 2 above the investigated absorption edge, prepared from micronized powder homogeneously mixed with micronized BN powder. The absorption spectra were measured within the interval from -250 eV to 1000 eV relative to the absorption edge. In the edge region the equidistant energy steps of 0.3 eV were used, while for the EXAFS region the equidistant k-steps ($\Delta k \approx 0.03$ Å^{-1}) were used with an integration time of 1 s/step. The EXAFS spectra were further analysed with the IFEFFIT program package [44].

To obtain the band gap excitation profiles and the band gap energies, diffuse reflectance spectra were recorded in the range from 250 to 800 nm with a UV-Vis spectrophotometer (Perkin Elmer, model λ 650S) equipped with a 150 mm integrated sphere and using spectralon as a reference material. According to the Kubelka-Munk theory [45], the diffuse reflectance data were converted to absorbance coefficients $F(R_\infty)$. $F(R_\infty) = (1-R)^2/2R = K/S$, where R, K and S are the reflectance, effective

absorption and scattering, respectively. The band gap (*Eg*) energies and absorption coefficients are related through the following relation [46]: $\alpha hv = A(hv - E_g)^{n/2}$, where α, hv and A are linear absorption coefficient, photon energy and proportionality constant, respectively. n = 1 for a direct band gap semiconductor or 4 for an indirect band gap semiconductor. Both $NdVO_4$ and $BiVO_4$ are direct band gap semiconductors so n = 1. Plotting the $[F(R_\infty)hv]^{1/n}$ against excitation energy allowed us to evaluate the band gap energy (the extrapolation of the linear part of the absorption edge on the photon energy axis gives the band gap energy).

Photoluminescence (PL) emission spectra are useful in determining the efficiency of charge carrier trapping, the migration and transfer, as well as in understanding the evolution of electron-hole pairs in semiconductors. The PL spectra were taken with a FLS920 Spectrometer of Edinburgh Instruments, using a steady state Xenon arc lamp. The experimental set-up was equipped with a blue sensitive high speed photomultiplier (Hamamatsu H5773-03 detector). The emission spectra were collected at room temperature, within 400-700 nm with an excitation wavelength of 371 nm.

3. Results and discussion

3.1. Structural analysis

3.1.1. X-ray powder diffraction

The XRD patterns in Fig. 1 show the formation of tetragonal $Bi_xNd_{1-x}VO_4$ solid solution for x between 0 and 0.48. When x > 0.48, two phase mixtures were obtained, which contained tetragonal $Bi_xNd_{1-x}VO_4$ and monoclinic $BiVO_4$. This shows that the solubility limit of Bi in $NdVO_4$ is between x=0.48 and 0.50. The crystallographic details of the $Bi_xNd_{1-x}VO_4$ samples, obtained after refinement of the unit cell, are presented in

Fig. 2. The standard deviation of the calculated unit cell parameters was ± 0.0002 Å. As the composition of the solid solution changes, the lattice constant also changes. We observed that the $NdVO_4$ unit cell volume decreased according to Vegard's law with the dopant concentration up to x = 0.48, while for higher concentrations, the unit cell volume remained constant. Thus, the solid solubility limit was found to be at x = 0.49(1).

The XRD patterns of $Nd_yBi_{1-y}VO_4$ (y < 0.08) compositions in Fig. 3 show the presence of only monoclinic $BiVO_4$ phase. For y ≥ 0.08, additional peaks of the tetragonal $NdVO_4$-based structure appear in the XRD pattern. The unit cell volume of this structure corresponds to the end member of the $Bi_xNd_{1-x}VO_4$ solid solution with x = 0.49(1). Because of very small dopant concentration and limited sensitivity of the XRD technique, we could not make convincing conclusions about the Nd substitution in $BiVO_4$ even for the y < 0.08 samples that appear to be single phase. Therefore, we have performed EXAFS studies to verify whether or not Nd^{3+}, in small concentrations enters the crystal structure of $BiVO_4$.

3.1.2. EXAFS study

3.1.2.1. Bi-doped $NdVO_4$

The XRD analysis on the Bi-doped $NdVO_4$ sample with $Bi_{0.2}Nd_{0.8}VO_4$ composition only showed the presence of tetragonal $NdVO_4$-based structure (space group I41/amd). To study distortion of the $NdVO_4$ local structure with the Bi-doping, we used EXAFS analysis–a chemically selective method that enables to study the crystallographic environment around Bi ions. Distinctive peaks in the Fourier transforms (FT) magnitude of the EXAFS spectra are contributions of the photoelectron backscattering on the near

neighbor shells around the central atom and represent the approximate radial distribution of the atoms surrounding the investigated central atom. The FT magnitude of k^2-weighted EXAFS spectra for Nd, Bi and V that were calculated over the range of k = 4–11 A^{-1} are compared in Fig. 4. Errors in FT magnitude EXAFS spectra due to the random noise in χ(k) are estimated at high R values (in the interval from 8–15 Å) and are of the order of ± $6 \cdot 10^{-3}$ for the Bi, ± $2 \cdot 10^{-2}$ for the Nd, and ± $4 \cdot 10^{-2}$ for the V spectrum. The qualitative comparison between the measured EXAFS signals shows that the Bi spectrum exhibits similar distribution of neighbour peaks as the Nd spectrum, and significantly different from the V one, suggesting that Bi ions in $Bi_{0.2}Nd_{0.8}VO_4$ have similar environment as Nd ions in $NdVO_4$. Such result was expected because the ionic radius of Bi^{3+} (1.17 Å) is similar to that of Nd^{3+} (1.11 Å), and much larger than that of V^{5+} (0.54 Å) [47]. It is therefore most unlikely that Bi^{3+} would replace V^{5+} in the $NdVO_4$ crystal lattice. The quantitative structural information on the local Bi neighbourhood in $Bi_{0.2}Nd_{0.8}VO_4$ and of Nd in $NdVO_4$ (type and average number of neighbour atoms and their distances from the selected atom, as well as the thermal or structural disorder of their positions - Debye-Waller factors) was obtained by Bi L_3-edge and Nd L_3-edge EXAFS analysis in which the model EXAFS function was fitted to the measured EXAFS spectrum. For that purpose we used FEFF6 computer code [48] to construct Nd model EXAFS functions *ab initio* from a set of scattering paths of the photoelectron, built from crystallographic data for $NdVO_4$ with $I4_1/amd$ space group (a = b = 7.33Å, c = 6.43 Å, α = β = γ = 90º [49]. In this crystal structure, the Nd atoms are surrounded by eight O atoms, four at the distance of 2.36 Å, and four at 2.64 Å. The second coordination sphere is occupied by two V atoms at 3.21 Å, followed by four V and four Nd atoms at 4.00 Å, and twelve O atoms at 4.4 Å.The Bi EXAFS model is

constructed from the same crystal structure with introduction of Bi on the Nd crystallographic site. All single and multiple scattering paths in the R range up to 4.09 Å were included in the models; in total 4 single scattering and 6 multiple scattering paths. A minimum number of variable parameters were introduced in the fits: a separate Debye-Waller factor (σ^2) and a common relative change of distances ($\Delta R/R$) for each shell of neighbours, except for the first shell where a separate ΔR was used. The common shift of the energy origin, ΔE_0, and the common amplitude reduction factor, S_0^2, were allowed to vary. In both models, the shell coordination numbers (N) were kept fixed at crystallographic values. The best-fit parameters are given in Table 1, and the quality of the fit is illustrated in Fig. 5 A and B. The error due to the random noise in $\chi(k)$ is $\pm 0.5 \cdot 10^{-4}$ and $\pm 1\ 10^{-3}$ for Bi and Nd spectrum, respectively. Errors in FT magnitude EXAFS spectra due to the random noise in $\chi(k)$ are estimated at high R values (in the interval from 8–15 Å) and are of the order of $\pm 6 \cdot 10^{-3}$ for Bi and $\pm 2 \cdot 10^{-2}$ for Nd spectrum. From the results of the Bi and Nd EXAFS analysis, we observed that the Bi neighbourhood in $Bi_{0.2}Nd_{0.8}VO_4$ is almost identical to that of Nd in $NdVO_4$. Only a small decrease (~2%) in the closest neighbour distances was found for Bi ions. These findings are consistent with the XRD study (see section 3.1.1) that showed a decrease in the unit cell volume of $Bi_xNd_{1-x}VO_4$ with Bi concentration. The smaller unit cell of $Bi_xNd_{1-x}VO_4$ as compared to $NdVO_4$ could be a consequence of the incorporation of Bi^{3+}cation with a stereochemically active lone electron pair.

3.1.2.2. Nd – doped $BiVO_4$

The XRD pattern of the sample with the nominal composition $Nd_{0.05}Bi_{0.95}VO_4$ corresponds to the single-phase monoclinic $BiVO_4$.We used the EXAFS analysis to

determine whether Nd has indeed entered the crystal structure of $BiVO_4$. We measured Nd L_3-edge EXAFS on the sample with the nominal composition $Nd_{0.05}Bi_{0.95}VO_4$, and V K-edge and Bi L_3-edge EXAFS on $BiVO_4$ sample. The FT of k^2-weighted Nd, Bi and V EXAFS spectra were calculated over the range of k = 3.5–10.5 $Å^{-1}$ Errors in FT magnitude EXAFS spectra due to the random noise in χ(k) are estimated at high R values (in the interval from 8–15 Å) and are of the order of $\pm 1 \cdot 10^{-3}$ for the Bi, $\pm 1 \cdot 10^{-2}$ for the Nd, and $\pm 3 \cdot 10^{-3}$ for the V spectrum.

The comparison between the measured FT EXAFS signals (Fig. 6) shows significant differences between the three spectra. Neither Bi nor V spectrum is similar to the Nd spectrum. This comparison strongly suggests that Nd in the sample with the nominal composition $Nd_{0.05}Bi_{0.95}VO_4$ does not have the same environment as Bi or V in $BiVO_4$. Therefore, Nd is probably forming a secondary phase with different local structure. Based on the described XRD studies it is reasonable to assume that the secondary phase is the $Bi_xNd_{1-x}VO_4$ end member, i.e. $Bi_{0.49}Nd_{0.51}VO_4$.

In order to fit the Nd EXAFS spectrum, we constructed Nd model EXAFS functions *ab initio,* from crystallographic data of the $NdVO_4$ reference [49], as described in the previous section (3.1.2), but in this case we substituted 50% of Nd neighbour atoms with Bi atoms, to obtain the EXAFS model for the $Bi_{0.5}Nd_{0.5}VO_4$ crystal structure. In the EXAFS model function all single and multiple scattering paths in the R range up to 5.1 Å were included. A minimum number of variable parameters were introduced in the fit: a separate Debye-Waller factor (σ^2) and a common relative change of distances ($\Delta R/R$), for each shell of neighbours, except for the first Nd-O distance and for the Nd-Bi distance where separate ΔR were used. The common shift of the energy origin, ΔE_0, and the common amplitude reduction factor S_0^2 were allowed to vary. The shell

coordination numbers (*N*) were kept fixed at the crystallographic values of the model $Bi_{0.5}Nd_{0.5}VO_4$ structure.

A very good fit of the experimental spectrum with the model $Bi_{0.5}Nd_{0.5}VO_4$ structure was obtained for the fitting performed in the *k* range from 3.4 $Å^{-1}$ to 10 $Å^{-1}$, and the *R* range from 1.35 Å to 5.1 Å. A complete list of the best-fit parameters is given in Table 2, and the quality of the fit is illustrated in Fig. 7. The error due to the random noise in $\chi(k)$ is $\pm 4 \cdot 10^{-3}$; and the error in FT magnitude EXAFS spectrum due to the random noise in $\chi(k)$ is estimated at high R values and is of the order of $\pm 1 \cdot 10^{-2}$.

From the parameters of the fit we can see that the local structure around Nd atoms in the sample with the nominal $Nd_{0.05}Bi_{0.95}VO_4$ composition is very similar to the local structure of Nd in $NdVO_4$ (see Table 1). However, we found that the Bi atoms are located at 0.3 Å larger distances as Nd atoms from the same shell. Also the distances to the oxygen atoms in more distant coordination shells are not the same as in the undoped $NdVO_4$, which indicates on some degree of structural distortion induced by the incorporation of Bi.

The results of the EXAFS analysis show that even for the smallest concentrations, Nd did not enter the crystal structure of $BiVO_4$ but it formed, most probably nanocrystalline, secondary $Bi_xNd_{1-x}VO_4$ phase with x = 0.49(1). The fact that Nd did not enter the $BiVO_4$ crystal structure is somewhat surprising, taking into account that the ionic radii of Nd^{3+} and Bi^{3+} are very similar (1.11 Å and 1.17 Å, respectively). The result indicates that for the stabilization of the $BiVO_4$ structure, the specific electron structure of Bi^{3+} is crucial. It appears that the hybridization of the Bi $6s^2$ and O 2p orbitals stabilizes the monoclinic $BiVO_4$ structure by distorting the Bi cation environment and adjusting the oxygen coordination sphere correspondingly. The

distance of the A-site ion to the first oxygen coordination sphere is shorter in the monoclinic $BiVO_4$ than in the tetragonal $NdVO_4$ (2.35 Å [50] and 2.44 Å, respectively) and, therefore, such cation site cannot be occupied by Nd^{3+} ion without the ability for the hybridization. This also explains why $NdVO_4$ and $BiVO_4$ crystallize in very different crystal structures and no Nd^{3+} can enter the A-site of $BiVO_4$. For the same reason no successful substitution on the A-site of the monoclinic $BiVO_4$ has been reported so far. $NdVO_4$ can adopt the monoclinic $BiVO_4$-type of structure but only under high pressure [39]. Such monoclinic structure with rare earth ions on the A-site is a metastable polymorph, in which, instead of the hybridization, the cation-oxygen distances are reduced by application of the external pressure.

3.2. Optoelectronic properties

3.2.1. Band gap analysis

The diffuse reflectance spectra of $Bi_xNd_{1-x}VO_4$ powders after the Kubelka-Munk treatment are presented in Fig. 8. The band gap of the single phase $NdVO_4$ was calculated to be 3.53 eV. This value is in the range of values reported in the literature (see Table 3), which significantly differ according to the morphology of the samples. From the Table 3 we can see a strong correlation of the particle size and the band gap values; smaller the particle size, smaller the band gap. Our result fits well into this trend. With introduction of Bi onto the A-site of $NdVO_4$, the band gap decreases from initial 3.53 eV to 3.06 eV for y = 0.40. In the lower concentration range, the influence of Bi on the band gap reduction is strong but becomes weaker for $x \geq 0.20$.

Taking in consideration the band structure of $BiVO_4$ and $NdVO_4$ [19,20,39], the observed red-shift of the $Bi_xNd_{1-x}VO_4$ band gap could be ascribed to the hybridization

between Bi $6s^2$ and O 2p orbitals on the top of the valence band of $NdVO_4$,which results in the up-shift of the valence band. This can be correlated with the colour change that we observed upon Bi doping, from blue-grey of $NdVO_4$ towards more yellowish green for $Bi_xNd_{1-x}VO_4$ as the Bi concentration increases.

The band gap energy of the monoclinic $BiVO_4$ obtained by us (~2.38 eV) is in a good agreement with values reported in the literature (~2.4 eV [15–17]). From Fig. 9 it can be seen that the band gap of $BiVO_4$ varies insignificantly with the nominal Nd concentration, which is consistent with the previous finding that Nd does not enter the crystal structure of $BiVO_4$.

The UV-vis spectra of $NdVO_4$, $Bi_xNd_{1-x}VO_4$ and $Bi_{0.49}Nd_{0.51}VO_4/BiVO_4$ composites show the presence of two different peaks centred at around 585 nm and 754 nm. These peaks (at the almost the same positions) have already been reported in the literature [51,53] and assigned to the electronic transitions of Nd^{3+} ion from $^4I_{9/2}$ to $^4G_{5/2}$ and from $^4I_{9/2}$ to $^4F_{7/2}$. This assignment is consistent with the fact that we have observed them for all the samples except for $BiVO_4$.

3.2.2. Photoluminescence properties

Photoluminescence spectra of the monoclinic $BiVO_4$ have been reported in the literature [15,22,29,38,54–56]. Most of the reported spectra show a broad peak in the range of 490-600 nm but with different intensity and peak position. These differences have been attributed to different synthesis method, particle size, and conditions of measurement (temperature, excitation wavelength etc). For example, $BiVO_4$ prepared by the ultrasonic method [56] showed a broad band from 490 until 570 nm, with three maxima.

The PL intensity of this sample was higher than the one of $BiVO_4$ obtained by the solid-state method. The sample prepared in an aqueous medium [29] showed a peak centred at about 600 nm with a higher intensity at 77 K than at room temperature, while in [15] no PL signal was observed, even at 83 K. The monoclinic $BiVO_4$, prepared by a liquid-solid reaction, gave a broad PL peak centred at about 715 nm [22]. Our spectrum of $BiVO_4$ (Fig. 10) looks similar to the spectrum reported for the ~20 nm sized $BiVO_4$ prepared via an ultrasound irradiation, measured at room temperature [55]. The broad peak in the emission spectrum of the $BiVO_4$ powder was attributed to a radiative recombination of the holes, formed in the O 2p of the valence band, with the $V3d^0$ electrons in the conduction band.

From Fig. 10 we see that the PL spectra of $BiVO_4$ and the nominal $Nd_yBi_{1-y}VO_4$ compositions have similar intensities (which is expected because Nd^{3+} does not enter the $BiVO_4$ structure). In the case of the nominal $Nd_yBi_{1-y}VO_4$ compositions, an additional peak can be observed at ~605 nm which could originate from the Nd^{3+} ion electronic transition (viz. $^4G_{7/2,9/2} \rightarrow {}^4I_{11/2,\ 13/2}$ [57]).

The PL spectra of $Bi_xNd_{1-x}VO_4$ powders are shown in Fig 11. Due to the electronic transitions inside the rare-earth ion (Nd^{3+}), the $NdVO_4$ spectrum shows more structures than the $BiVO_4$ one. The nature of these transitions can be understood based on Judd-Ofelt theory [58]. In the tetragonal $NdVO_4$, the Nd^{3+} ions are located at the sites that lack the centre of symmetry (D_{2d} symmetry) [39,59] which makes the electronic dipole transitions within the Nd^3 4f shells possible. Calculation of the energy level diagrams for Nd^{3+} in $NdVO_4$ can be found in [59]. The PL properties of $NdVO_4$ upon UV excitation have so far been reported only for single-crystalline nanorods, measured with an excitation wavelength of 310 nm at room temperature [53]. The sharp emission

bands in the wavelength range 350–500 nm, detected on the $NdVO_4$ nanorods, are not present in the PL spectrum that we have recorded on the powders with around 1μm particle size, but we observed similar emissions in the interval of 500 - 650 nm as reported in [53,57,60,61]. Therefore, the emission peaks at ~503, 525, 556, 598, and 605-612 nm could be assigned to the $^4G_{11/2} \rightarrow {}^4I_{11/2}$ [57], $^4G_{7/2} \rightarrow {}^4I_{9/2}$ [60,61], $^4G_{9/2} \rightarrow {}^4I_{9/2}$[53,61], $^4G_{5/2} \rightarrow {}^4I_{9/2}$ and $^4G_{7/2,\ 9/2} \rightarrow {}^4I_{11/2,\ 13/2}$ transitions respectively [57].

PL spectrum lineshape of $Bi_xNd_{1-x}VO_4$ changes with respect to the spectrum of $NdVO_4$, but the intensity and lineshape of PL spectra of $Bi_xNd_{1-x}VO_4$ solid solutions do not change with the Bi concentration. There is a decrease of the emission intensity in the range of 425–600 nm with the appearance of sharp peaks at about 500 and 525 nm and a broad band with a maximum at about 545 nm. Moreover, in the range of 650–675 nm, a new triplet is clearly visible in the PL spectra of $Bi_xNd_{1-x}VO_4$ solid solutions. The fact that the new triplet appeared only in $Bi_xNd_{1-x}VO_4$ ($x > 0$) samples and not in the $BiVO_4$ or $NdVO_4$ spectra, shows that these new emissions are caused by the small modifications of the Nd^{3+} local structure in $NdVO_4$ with the Bi^{3+} doping (see section 3.1.2).

4. Conclusions

The phase relations and optoelectronic properties in the $BiVO_4$-$NdVO_4$ system have been reported. We have found that Bi substitutes Nd according to formula $Nd_{1-x}Bi_xVO_4$ up to $x = 0.49(1)$. The EXAFS study of Bi in the $Bi_{0.2}Nd_{0.8}VO_4$ sample showed that the first oxygen atoms around Bi^{3+} are at a smaller distance as it could be expected from their ionic radii, which is a consequence of the hybridization of Bi $6s^2$ and O 2p orbitals. By the Bi-doping, we succeeded to shift the absorption of $NdVO_4$ towards the visible

range of the solar spectrum and, so, to enhance its optical absorption. The decrease of the band gap has been attributed to the Bi $6s^2$ - O 2p hybridization at the top of the $NdVO_4$ valence band. This is also in agreement with the observed reduction in the unit cell volume with the increase in concentration of the larger Bi^{3+} ion (increasing x) and the appearance of new emission lines in the PL spectra. On the other side of the $BiVO_4$-$NdVO_4$ system, Nd does not substitute either Bi or V in the $BiVO_4$ structure.

Acknowledgements

The XAS experiments were performed at beamline C of HASYLAB at DESY, Hamburg (project I-20110082 EC). The work has been supported by the Slovenian Research Agency research programme P1-0112 and P2-0337, Centre of Excellence Low-Carbon Technologies (CO NOT) Slovenia, and by DESY and the European Community's Seventh Framework Programme (FP7/2007-2013) under grant agreement CALIPSO n° 312284.".We would like to thank Roman Chernikov and Edmund Welter of HASYLAB, for support and expert advice on beamline operation.

References

[1] van de Krol R, Liang Y, Schoonman J. J Mater Chem 2008;18:2311.

[2] Tong H, Ouyang S, Bi Y, Umezawa N, Oshikiri M, Ye J. Adv Mater 2012;24:229.

[3] Fujishima A, Honda K. Nature 1972;238:37.

[4] Chen X, Mao SS. Chem Rev 2007;107:2891.

[5] Wagner FT, Somorjai GA. Nature 1980;285:559.

[6] Reiche H, Dunn WW, Bard AJ. J Phys Chem 1979;83:2248.

[7] Chen X, Liu L, Yu PY, Mao SS. Science 2011;331:746.

[8] Chen X, Li P, Tong H, Kako T. Sci Technol Adv Mater 2011;12:044604.

[9] Kim W, Tachikawa T, Majima T, Choi W. J Phys Chem C 2009;113:10603.

[10] Kudo A, Ueda K, Kato H, Mikami I. Catal Lett 1998;53:229.

[11] Zhang L, Chen D, Jiao X. J Phys Chem B 2006;110:2668.

[12] Bhattacharya AK, Mallick KK, Hartridge A. Mater Lett 1997;30:7.

[13] Stoltzfus MW, Woodward PM, Seshadri R, Klepeis JH, Bursten B. Inorg Chem 2007;46:3839.

[14] Tokunaga S, Kato H, Kudo A. Chem Mater 2001;13:4624.

[15] Kudo A, Omori K, Kato H. J Am Chem Soc 1999;121:11459.

[16] Yao W, Ye J. J Phys Chem B 2006;110:11188.

[17] Jo WJ, Jang WJ, Kong K, Kang HJ, Kim JY, Jun H, Parmar KPS, Lee JS. Angew Chem, Int Ed 2012;51:3147.

[18] Zhao Z, Li Z, Zou Z. Phys Chem Chem Phys 2011;13:4746.

[19] Payne DJ, Robinson M, Egdell RG, Walsh A, McNulty J, Smith KE, Piper LFJ. Appl Phys Lett 2011;98:212110.

[20] Walsh A, Yan Y, Huda MN, Al-Jassim MM, Wei SH. Chem Mater 2009;21:547.

[21] Xi G, Ye J. Chem Commun 2010;46:1893.

[22] Sasaki Y, Nemoto H, Saito K, Kudo A. J Phys Chem C 2009;113:17536.

[23] Yu J, Kudo A. Adv Func Mater 2006;16:2163.

[24] Ge L. J Mol Catal A: Chem 2008;282:62.

[25] Ge L. Mater Lett 2008;62:926.

[26] Cao SW, Yin Z, Barber J, Boey FYC, Loo SCJ, Xue C. ACS Appl Mater Interfaces 2012;4:418.

[27] Zhou B, Zhao X, Liu H, Qu J, Huang CP. Sep and Purif Technol 2011;77:275.

[28] Zhou B, Zhao X, Liu H, Qu J, Huang CP. Appl Catal, B 2010;99:214.

[29] Long M, Cai W, Cai J, Zhou B, Chai X, Wu Y. J Phys Chem B 2006;110:20211.

[30] Liang L, Luo X, Lin X, Xu C, Zhao Z. Mater Sci Forum 2009;620-622:655.4

[31] Zhang A, Zhang J. Acta Phys -Chim Sin 2010;26:1337.

[32] Weifeng Y, Hideo I, Jinhua Y. Dalton Trans 2008;11:1426.

[33] Liang Y, Tsubota T, Mooij LPA, van de Krol R. J Phys Chem C 2011;115:17594.

[34] Bi J, Li J, Wu L, Zheng H, Su W. Mater Res Bull 2012;47:850.

[35] Neves M C, Lehocky M, Soares R, Lapcik LJr, Trinidade T. Dyes Pigm 2003;59:181.

[36] Xu H, Wu C, Li H, Chu J, Sun G, Xu Y, Yan Y. Appl Surf Sci 2009;256:597.

[37] Zhang A, Zhang J. J Hazard Mater 2010;173:265.

[38] Zhang A, Zhang J. Chin J Chem Phys 2010;23:73.

[39] Panchal V, Errandonea D, Segura A, Rodriguez-Hernandez P, Munoz A, Lopez-Moreno S, Bettinelli M. J Appl Phys 2011;110:043723.

[40] Mahapatra S, Madras G, Row TNG. Ind Eng Chem Res 2007;46:1013.

[41] Di Paola A, Garcia-Lopez E, Marci G, Palmisano L. J Hazard Mater 2012;211-212:3.

[42] Mahapatra S, Nayak SK, Madras G, Row TNG. Ind Eng Chem Res 2008;47:6509.

[43] Mahapatra S, Vinu R, Row TNG, Madras G. Appl Catal, A 2008;351:45.

[44] Ravel B, Newville M. J Synchrotron Radiat 2005;12:537.

[45] Kubelka P, Munk F. Zeitschr f Techn Physik 1931;12:593 (in German).

[46] Butler MA. J Appl Phys 1977;48:1914.

[47] Shannon RD. Acta Crystallogr A 1976;A32:751.

[48] Rehr JH, Albers RC, Zabinsky SI. Phys Rev Lett 1992;69:3397.

[49] Milligan WO, Vernon LW. J Phys Chem 1952;56:145.

[50] Sleight AW, Chen H, Ferretti A, Cox DE. Mater Res Bull 1979;14:1571.

[51] Xu J, Hu C, Liu G, Liu H, Du G, Zhang Y. J Alloys Compd 2011;509:7968.

[52] Kalai Selvan R, Gedanken A, Anilkumar P, Manikandan G, Karunakaran C. J Cluster Sci 2009;20:291.

[53] Wu X, Tao Y, Dong L, Zhu J, Hu Z. J Phys Chem B 2005; 109:11544.

[54] Liu W, Yu Y, Cao L, Su G, Liu X, Zhang L, Wang Y. J Hazard Mater 2010;181:1102.

[55] Yu C, Yang K, Yu CJ, Cao F, Zhou X. J Alloys Compd 2011;509:4547.

[56] Shang M, Wang W, Zhou L, Sun S, Yin W. J Hazard Mater 2009;172:338.

[57] Balda R, Fernandez J, Nyein EE, Hommerich U. Opt Express 2006;14:3993.

[58] Walsh MB. Judd-Ofelt Theory: Principles and Practices, in: Di Bartolo B, Forte O (Eds.). Advances in Spectroscopy for Lasers and Sensing. The Netherlands: Springer, 2006.

[59] Antic-Fidancev E, Holsa J, Lemaitre-Blaise M, Porcher P. J Phys: Condens Matter 1991;3:6829.

[60] Deng H, Yang S, Xiao S, Gong HM, Wang QQ. J Am Chem Soc 2008;130:2032.

[61] Peng XN, Zhang X, Yu L, Zhou L. Mod Phys Lett B 2009;23:2647.

Figure captions

Fig. 1. X-ray diffraction patterns of Bi-doped $NdVO_4$ samples with the nominal stoichiometry $Bi_xNd_{1-x}VO_4$. The filled circles denote the tetragonal $NdVO_4$ phase (space group $I4_1/amd$), while the filled triangles represent the monoclinic $BiVO_4$ phase.

Fig. 2. Unit cell variation of $Bi_xNd_{1-x}VO_4$ samples as a function of Bi concentration (x).

Fig. 3. X-ray diffraction patterns of Nd-doped $BiVO_4$ samples with the nominal stoichiometry $Nd_yBi_{1-y}VO_4$. The tetragonal $NdVO_4$-based phase is represented with the crosses, while the monoclinic $BiVO_4$ phase is represented with the filled circles.

Fig. 4. Magnitude of Fourier transforms of the k^2-weighted Bi L_3-edge EXAFS of $Bi_{0.2}Nd_{0.8}VO_4$, Nd L_3-edge of $NdVO_4$ and V K-edge in $BiVO_4$ calculated in the k range of 4–11 $Å^{-1}$.

Fig. 5. (A) The k^2-weighted Bi and Nd L_3-edge EXAFS spectra (dots) and best fit EXAFS models (solid line). (B) Fourier transforms magnitude of k^2-weighted Bi L_3-edge EXAFS in $Bi_{0.2}Nd_{0.8}VO_4$ and of Nd L_3-edge EXAFS in $NdVO_4$ (solid lines), compared to their best fit EXAFS models (red dashed line) calculated in the R range = 1–4 Å (spectra are shifted for clarity).

Fig. 6. Fourier transform magnitude of the k^2-weighted Nd L_3-edge EXAFS measured on the sample with the $Nd_{0.05}Bi_{0.95}VO_4$ nominal composition, compared to k^2-weighted Bi L_3-edge and V K-edge FT EXAFS spectra, measured on $BiVO_4$ calculated in the k range of 3.5–10.5 $Å^{-1.}$

Fig. 7 (A) The k^2-weighted Nd L_3-edge EXAFS spectrum, measured on the sample with the $Nd_{0.05}Bi_{0.95}VO_4$ nominal composition (dots), and its best fit EXAFS model (solid line). (B) Fourier transforms magnitude of the k^2-weighted Nd L_3-edge EXAFS spectrum (solid line), measured on the sample with the $Nd_{0.05}Bi_{0.95}VO_4$ nominal composition, compared to the best fit EXAFS model (dashed line) calculated in the R range = 1.35–5.1 Å

Fig. 8. UV-Vis diffuse reflectance spectra of $Bi_xNd_{1-x}VO_4$ with x = 0, 0.1, 0.2, 0.3, and 0.4. The Kubelka-Munk function is plotted versus the excitation energy. The band gap

(Eg) of $NdVO_4$ decreased by Bi-doping. The insert shows the band gap determination of $NdVO_4$.

Fig. 9. UV-Vis diffuse reflectance spectra of nominal $Nd_yBi_{1-y}VO_4$ compositions. The Kubelka-Munk function is plotted versus the excitation energy. The Eg of $BiVO_4$ varies insignificantly with Nd concentration. The insert shows the band gap determination of $BiVO_4$.

Fig. 10. Room temperature PL spectra of $BiVO_4$ and nominal $Nd_yBi_{1-y}VO_4$ compositions.

Fig. 11. Room temperature PL spectra of $Bi_xNd_{1-x}VO_4$ powders.

*Text only
Click here to view linked References

Table captions

Table 1

Structural parameters of the first coordination shells around Bi atom in $Bi_{0.2}Nd_{0.8}VO_4$ and around Nd in $NdVO_4$, respectively. *R* = distance and σ^2 = Debye-Waller factor. Uncertainty of the last digit is given in parentheses. The fitting statistics *R-factor* was 0.0018 for the Bi fit and 0.005 for the Nd fit. The amplitude reduction factor was S_0^2= 0.98 ± 0.09 for Bi and 0.94 ± 0.07 for Nd. The shift of the energy origin, ΔE_0 was -4 ± 1 eV for Bi and 3.7 ± 0.8 eV for Nd.

Neighbour element of		Number of neighbours of		R [Å]		σ^2 [Å^2]	
Bi in $Bi_{0.2}Nd_{0.8}VO_4$	Nd in $NdVO_4$	Bi in $Bi_{0.2}Nd_{0.8}VO_4$	Nd in $NdVO_4$	From Bi in $Bi_{0.2}Nd_{0.8}VO_4$ to	From Nd in $NdVO_4$ to	Bi in $Bi_{0.2}Nd_{0.8}VO_4$ to	Nd in $NdVO_4$ to
O		8		2.39(1)	2.44(1)	0.019(1)	0.010(1)
V		2		3.20(1)	3.22(1)	0.008(1)	0.004(1)
Nd		4		3.99(1)	4.00(1)	0.013(1)	0.008(1)
V		4		3.99(1)	4.00(1)	0.016(1)	0.010(1)

Table 2

Structural parameters of the first coordination shells around Nd atom in the $Bi_{0.5}Nd_{0.5}VO_4$ model structure. R = distance and σ^2 = Debye-Waller factor. Uncertainty of the last digit is given in parentheses. The fitting statistics, *R-factor*= 0.007. The amplitude reduction factor $S_0^2 = 0.8 \pm 0.1$, and the shift of the energy origin $\Delta E_0 = 1.3 \pm 1.5$ eV.

Neighbour element of Nd	Number of neighbours	R [Å]	σ^2 [Å^2]
O	8	2.43(1)	0.008(1)
V	2	3.15(2)	0.007(2)
Nd	2	3.92(2)	0.003(2)
V	4	3.92(2)	0.011(2)
Bi	2	4.22(3)	0.003(2)
O	12	4.31(2)	0.015(5)
O	8	5.06(7)	0.011(1)

Table 3

Experimental band-gap energy values for $NdVO_4$.

Paper	Experimental Eg [eV]	Synthesis method and particle size
Panchal V et al. [39]	3.72	Single crystals, ~ 80μm
This work	3.53	Solid-state synthesis, ~1 μm
Mahapatra S et al. [40]	2.99	Co-precipitation, 200 nm particles
Xu J et al. [51]	2.95	Molten salt method, 100 nm diameter and up to 3 μm length nanowires
Kalai Selvan R et al. [52]	2.15	Sonochemical synthesis, 20 nm rods

Figure(s)

Click here to download high resolution image

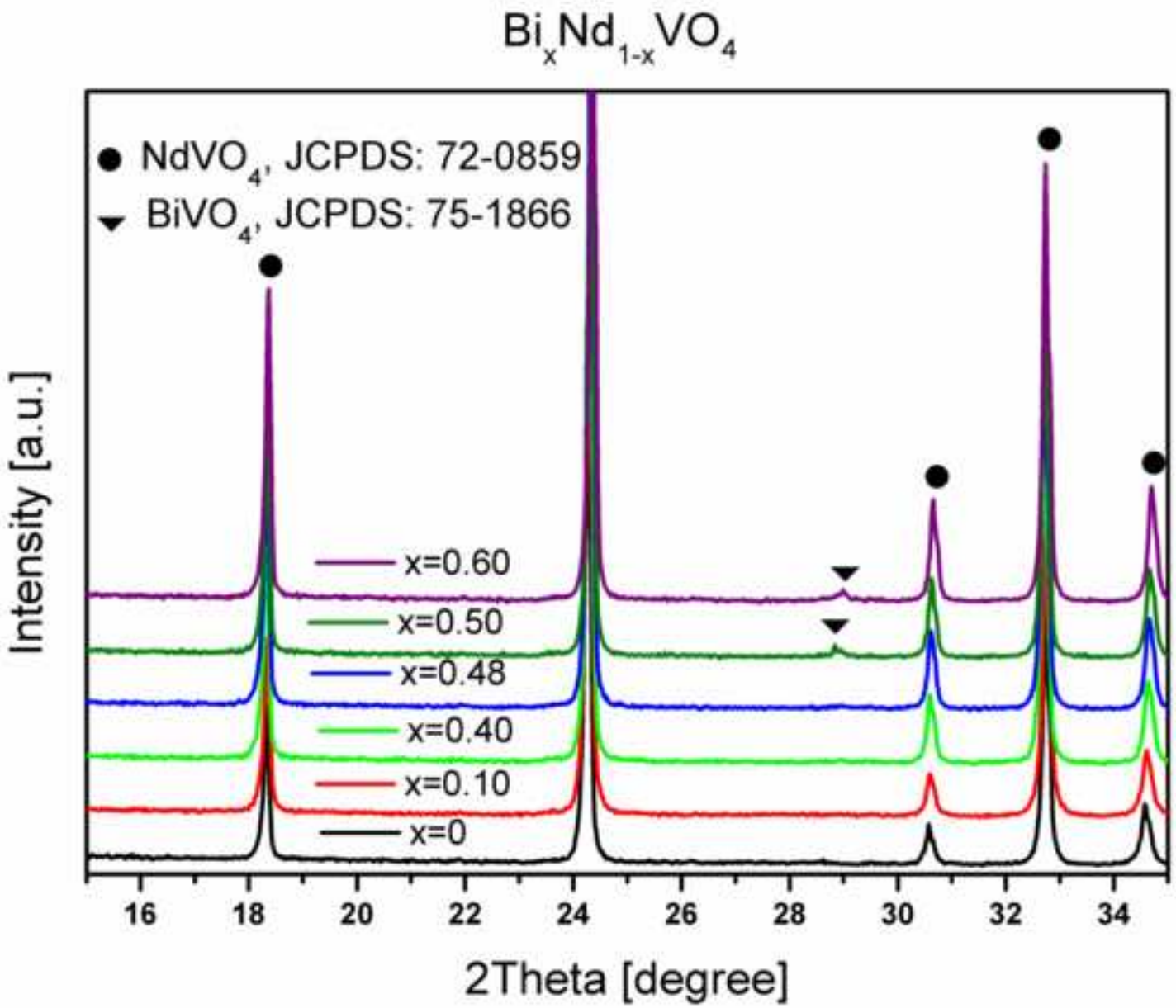

Figure(s)

Click here to download high resolution image

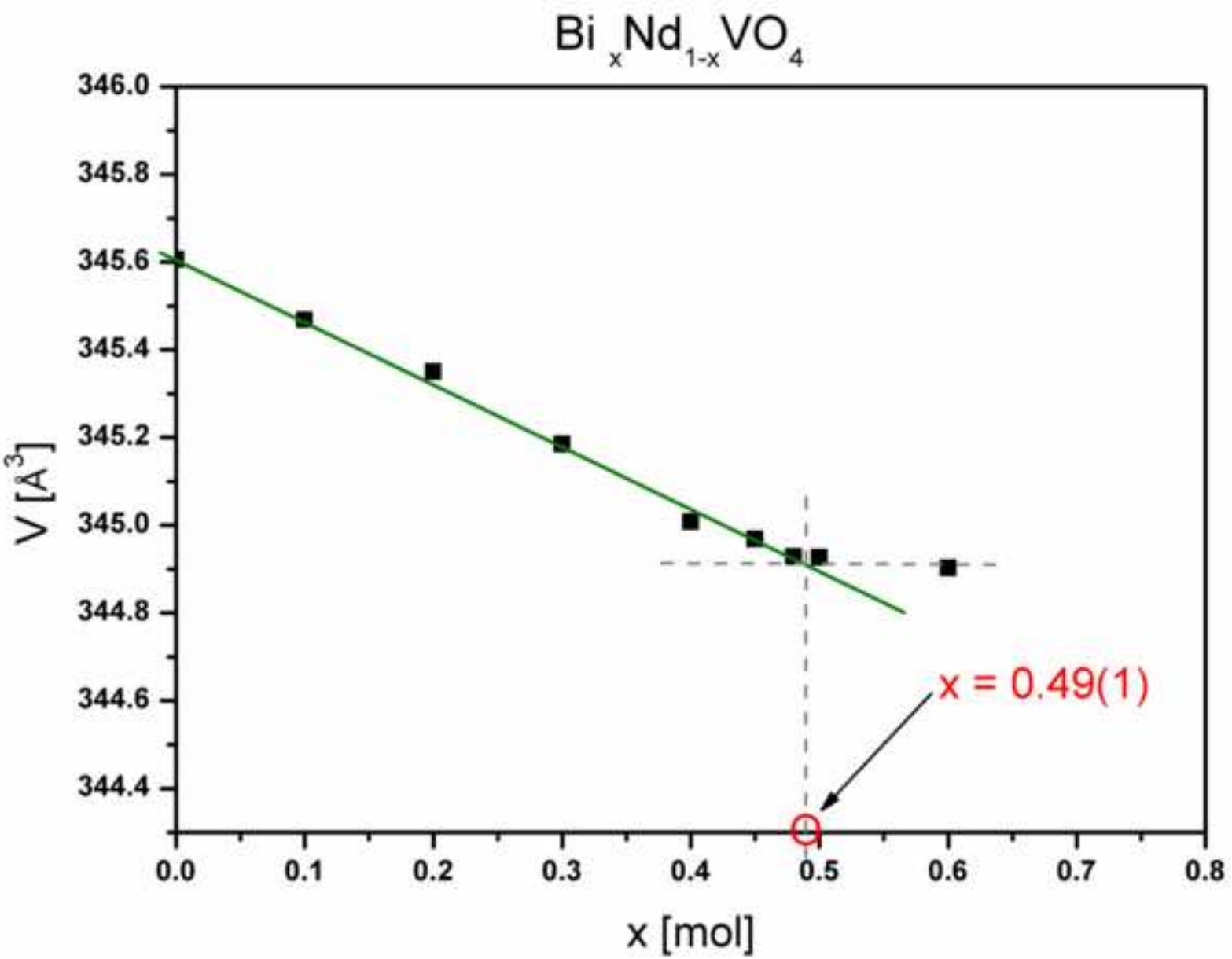

Figure(s)

Click here to download high resolution image

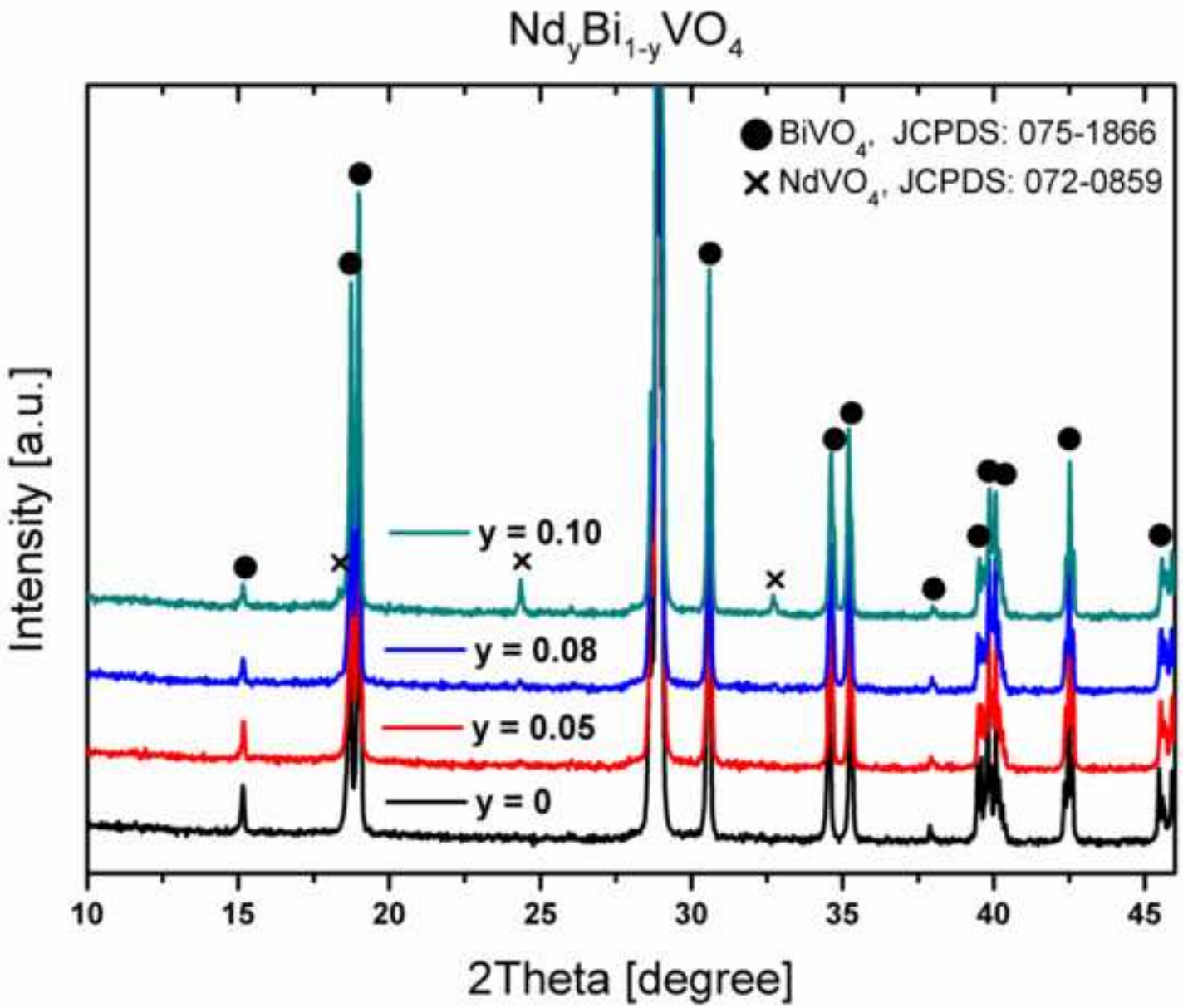

Figure(s)

Click here to download high resolution image

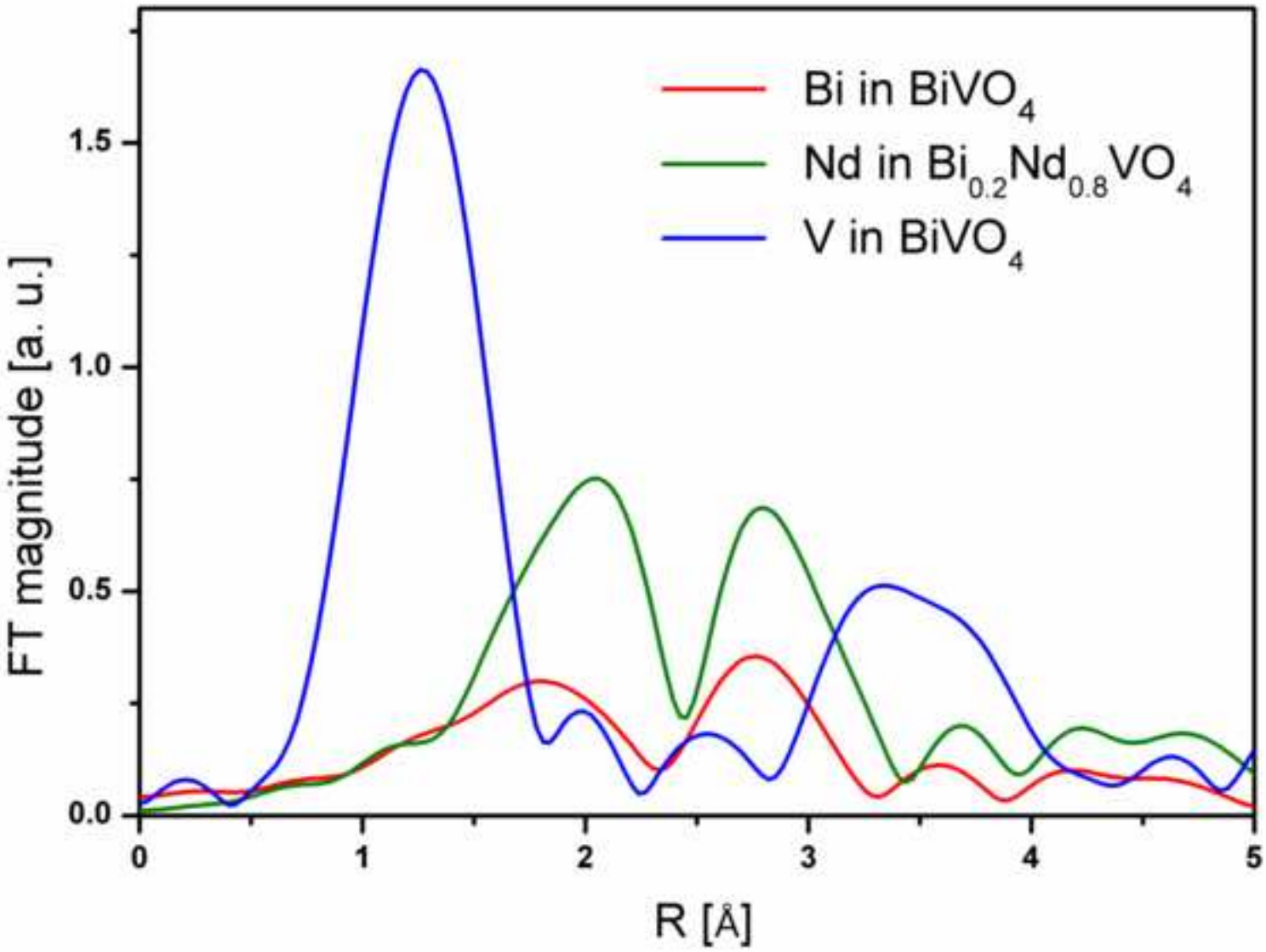

Figure(s)

Click here to download high resolution image

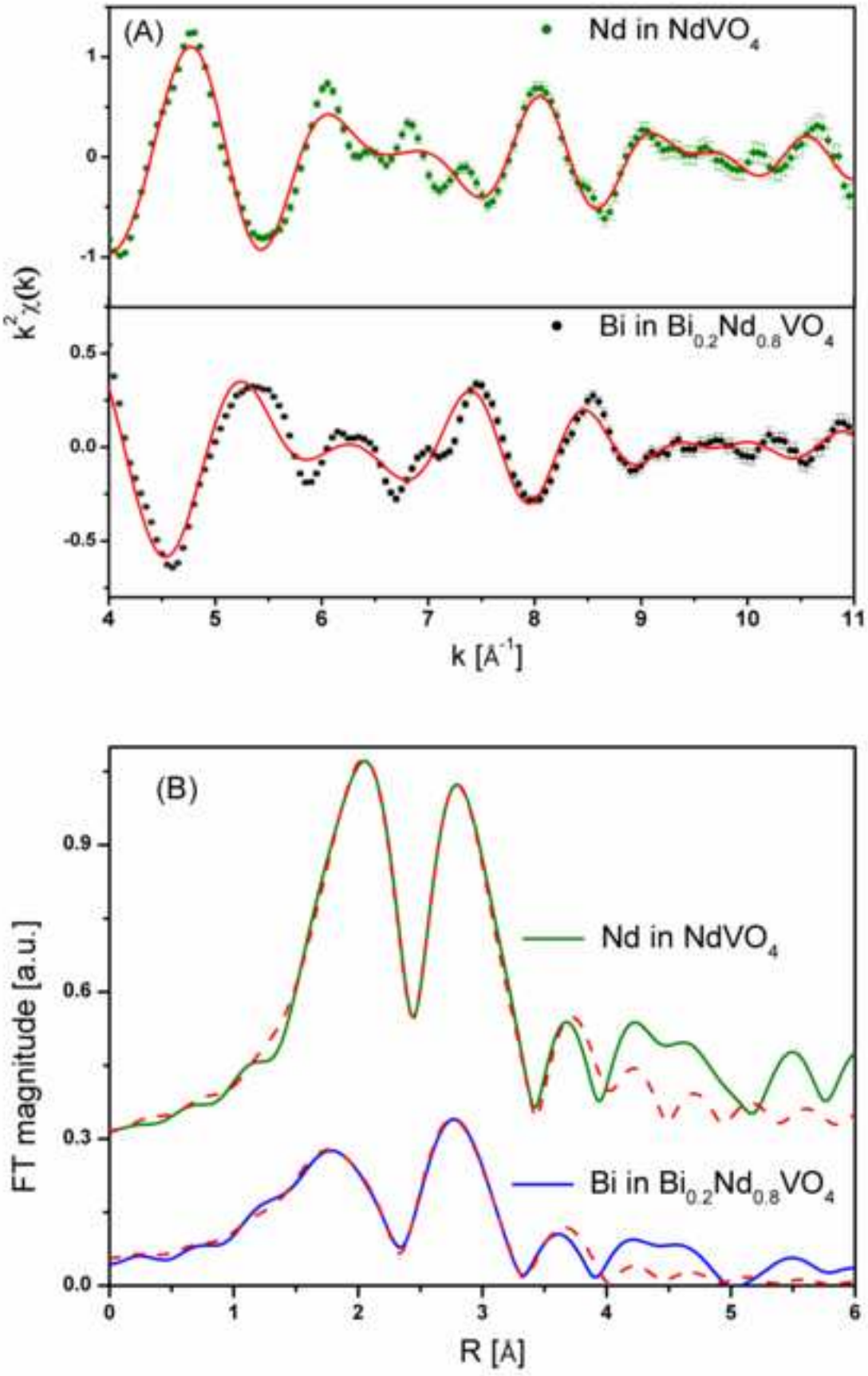

Figure(s)

Click here to download high resolution image

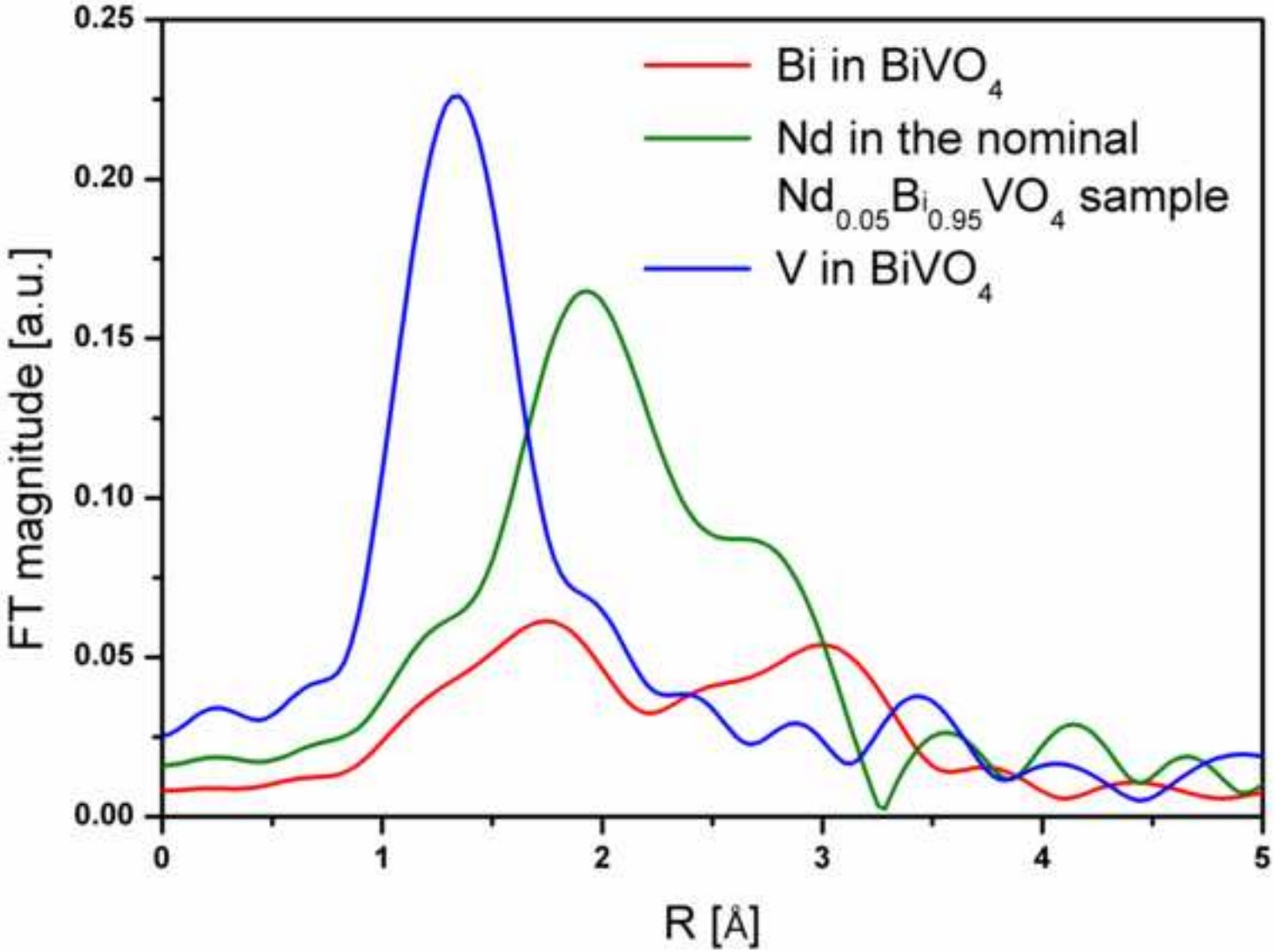

Figure(s)

Click here to download high resolution image

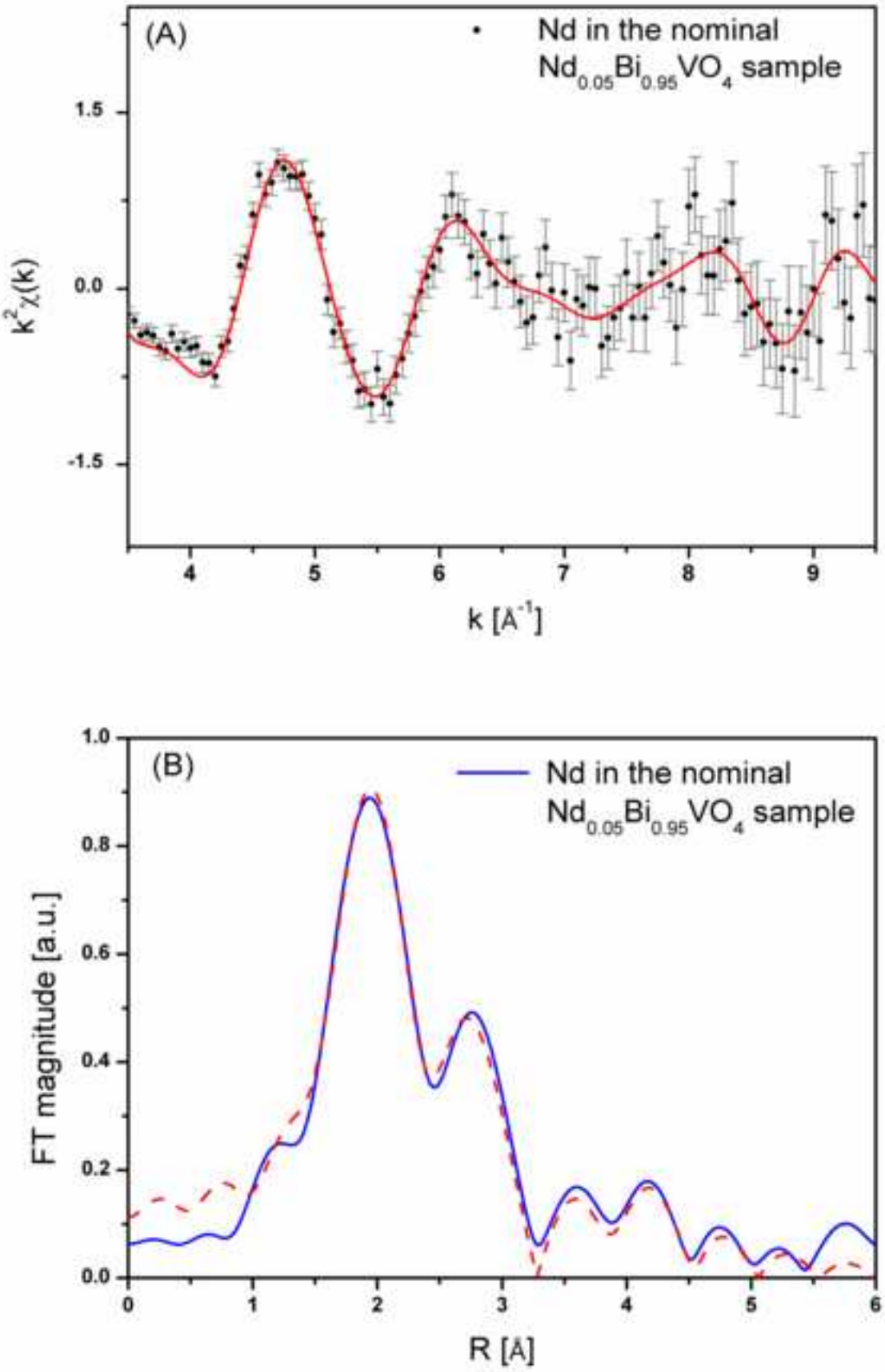

Figure(s)

Click here to download high resolution image

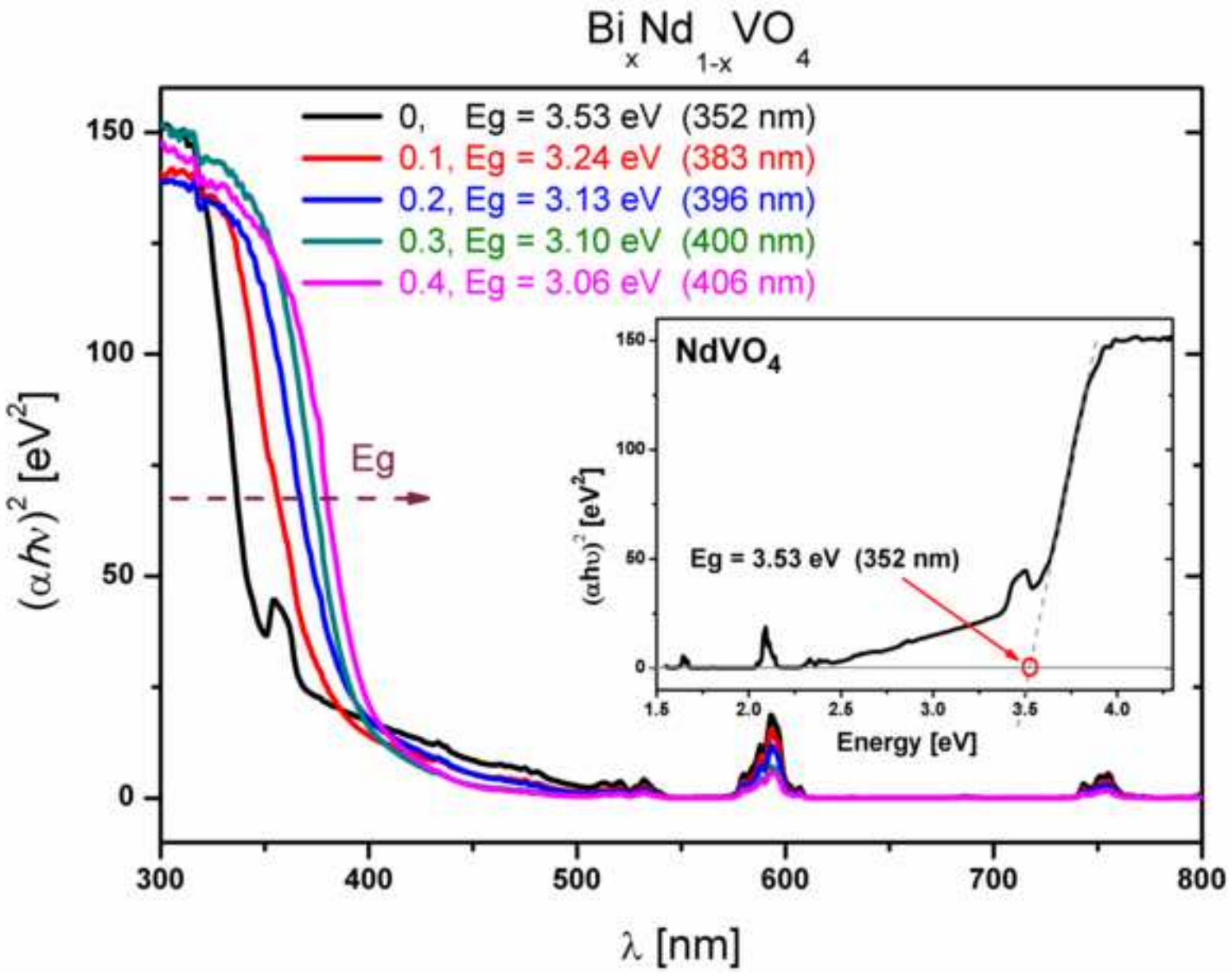

Figure(s)

Click here to download high resolution image

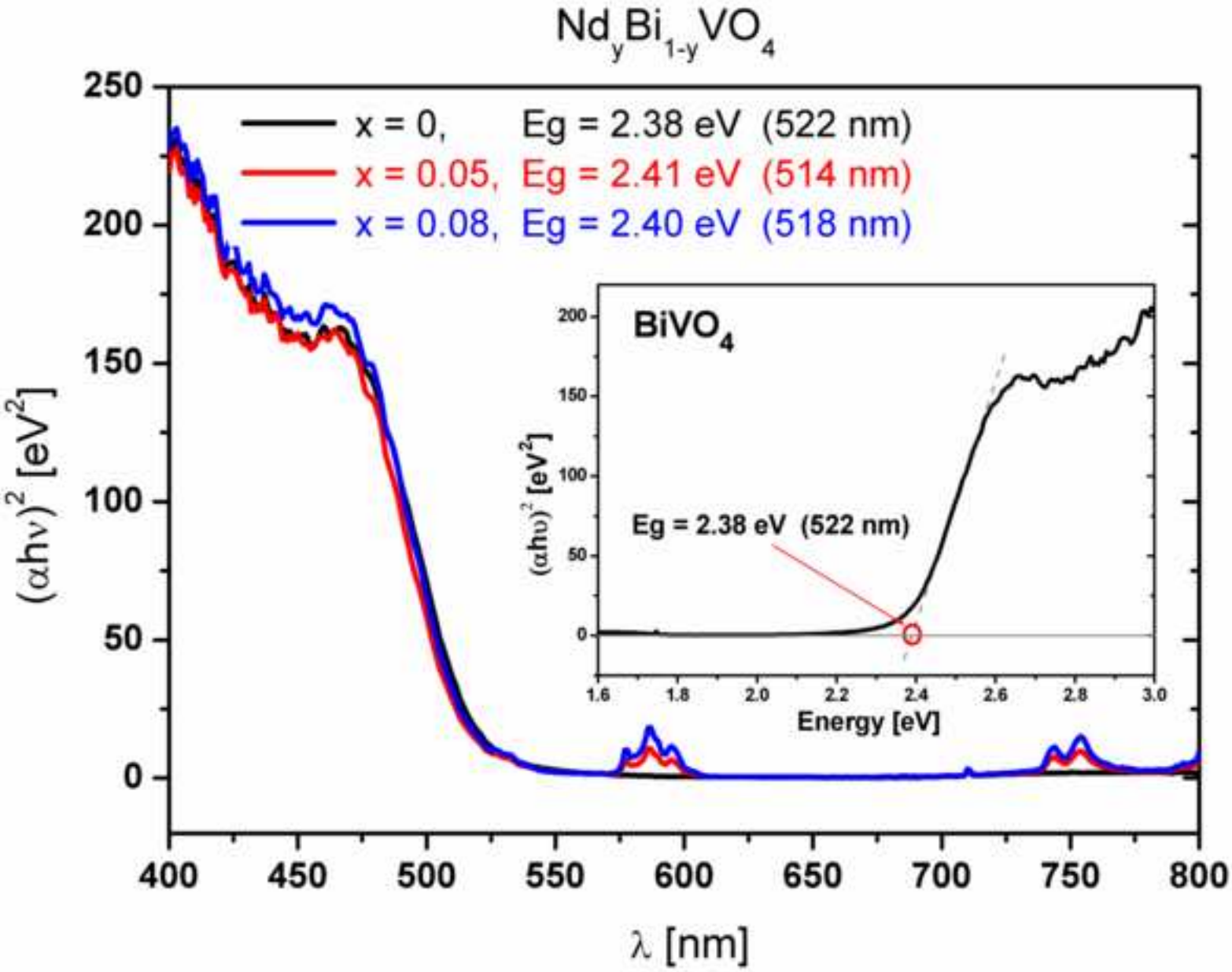

Figure(s)

Click here to download high resolution image

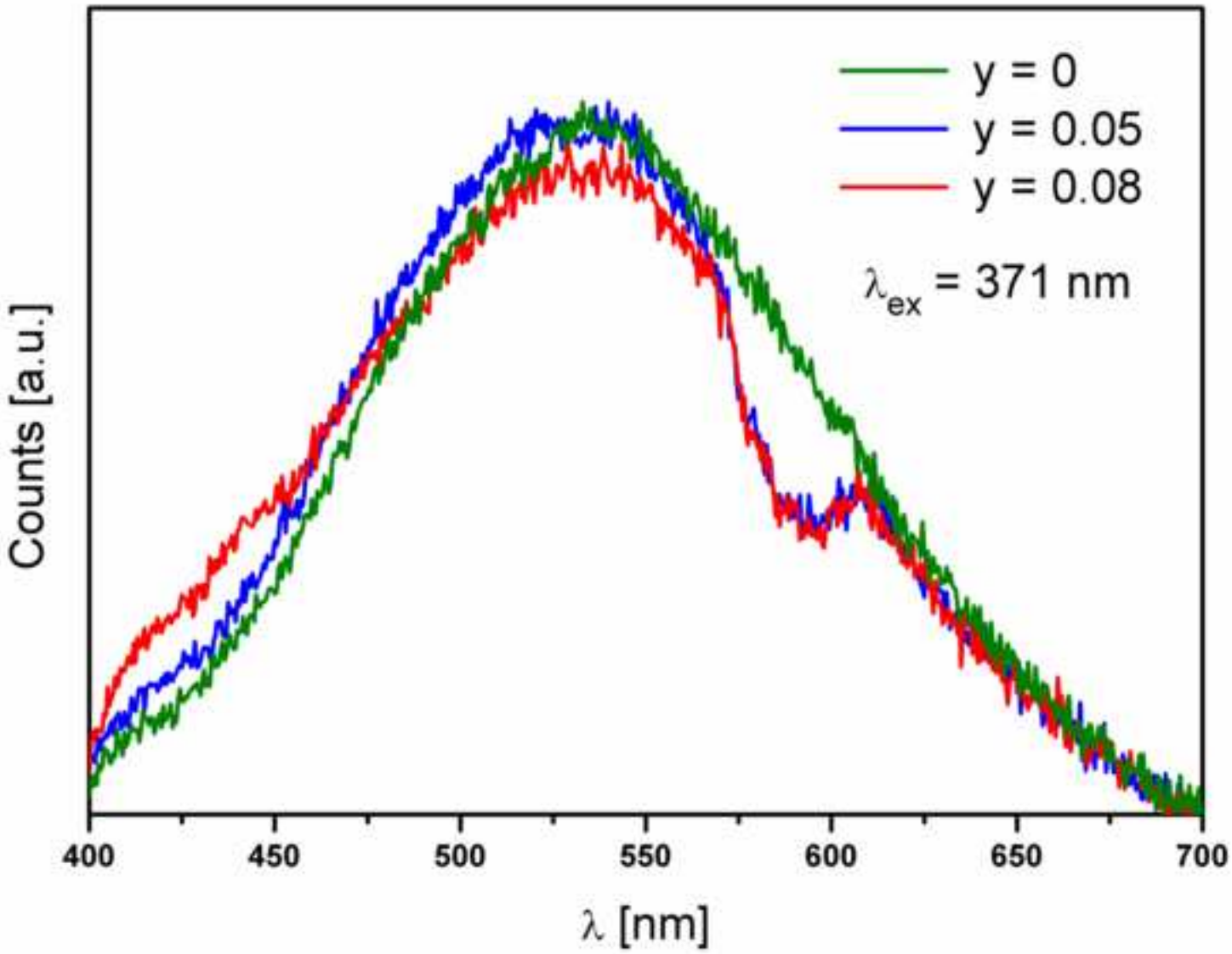

Figure(s)

Click here to download high resolution image